# Photochemistry of Molecules at Confined Environment: $CD_3Br/O/Ru(001)$ and $CO_2$@Ice

RAPHAEL BERGER,[a] YIGAL LILACH,[b] YOUSIF AYOUB,[a] AND MICHA ASSCHER[a,]*
[a]Department of Physical Chemistry and the Farkas Center for Light-Induced Processes, The Hebrew University of Jerusalem, Jerusalem 91904, Israel
[b]Department of Chemistry and Biochemistry, University of California, Santa Barbara, Santa Barbara, California 93106, USA

*(Received 14 May 2004 and in revised form 17 June 2004)*

**Abstract.** The photochemistry of molecules constrained within a confining environment on surfaces has been studied. Orientation of methyl bromide could be controlled methyl down or up by varying the pre-adsorbed oxygen coverage due to electrostatic interactions on Ru(001) under UHV conditions. Irradiation of the coadsorption system at 193 nm has shown that the resulting photochemical activity is sensitive to the molecular orientation. Photodesorption and dissociation cross sections were $1.0 \cdot 10^{-19}$ $cm^{-2}$ for methyl-down and $3.0 \cdot 10^{-19}$ $cm^{-2}$ for the methyl-up configurations. This observation represents the first report of the steric effect in electron–molecule interaction due to the dissociative electron attachment mechanism of photochemical processes on surfaces.

A second system of $CO_2$ molecules caged within ice has also been studied. Here the trapped carbon dioxide molecules cannot leave the surface at their normal desorption temperature near 100 K, but are explosively desorbing at the onset of ice evaporation near 165 K. Upon UV irradiation, enhanced dissociation to adsorbed CO and oxygen is recorded. In addition, a new reactivity channel is observed to form $H_2CO$, tentatively identified as formaldehyde. The relevance of photochemistry of caged molecules within ice to interstellar hydrocarbon formation as a possible route for the origin of life is discussed.

## 1. INTRODUCTION

Chemical reactivity of molecules at constrained environment has been the focus of extensive research in recent years. The role of solid and liquid surroundings in orienting molecules, restricting some reactivity channels while enhancing others, is the basis for selectivity that is particularly important in heterogeneous catalysis and biology. Proper mutual orientation of reactants has been realized to be almost as important as energetic requirements for a successful reactive encounter. One experimental approach to the study of molecular orientation-dependent reactivity has been via molecular beam studies in the gas phase, a focus of interest more than a decade ago. In these studies, electrostatic hexapole technology was employed to orient gas phase molecules in a beam and then let them collide with alkali metals[1–4] and other electron donor (reducing) atoms.[5] In cases such as those of methyl halides, the halogen side was found to be more reactive than the methyl tail.[2,5]

Electron–molecule interactions (electron transfer processes) have been the focus of basic science interest in both chemistry and biology for decades. Studies in this field have included inter- and intra-molecular electron transfer,[6] transmission[7–9] conduction within and through molecular layers,[10–11] and dissociative electron attachment (DEA) processes.[12–14] Recent interest in molecular electronics has brought the basic science in this field closer to modern technology than ever before.[8–10]

Based on the extensive research discussed above, it is interesting and surprising to note that in spite of the tremendous importance of electron-induced processes in chemical and biological systems, previous studies

*Author to whom correspondence should be addressed. E-mail: asscher@fh.huji.ac.il

have not attempted to directly investigate molecular orientation dependence or stereochemistry in electron–molecule interactions.

Here we introduce and demonstrate the effect of molecular orientation on electron–molecule interaction. Specifically, by tuning the oxygen coverage on ruthenium, the orientation of methyl bromide could be controlled bromine down or methyl down on O/Ru(001). Tuned electrostatic interactions by the surrounding oxygen-covered surface were used to orient adsorbed molecules and consequently affect their (photo) reactivity. Similar behavior was reported in the co-adsorption system of potassium with water on Pt(111).[15,16] The other example of the effect of surrounding molecules on (photo) reactivity will be that of caged $CO_2$ within amorphous solid water on clean Ru(001) – $CO_2$@Ice.

## 2. EXPERIMENTAL

The photochemistry experiments described below were performed in an ultra high vacuum (UHV) apparatus, described elsewhere in detail.[19] It is equipped with LEED/Auger, a quadrupole mass spectrometer (QMS) for temperature programmed desorption (TPD) and for real-time detection of desorbing molecules during laser irradiation and electron bombardment. Adsorbates orientation could be determined by means of a Kelvin probe, operated in a differential Δφ-TPD mode, as explained elsewhere in detail.[19] A mini excimer laser was operated at 193 nm, 1 mJ/pulse, 10-ns pulse duration at a variable repetition rate up to 100 Hz. Low energy electrons at 10 eV kinetic energy bombarded the adsorbate system via a retarding grid that decreased the electrons' energy from 100 eV at a typical sample current of 0.1 μA. The Ru(001) sample, oriented to within 0.1 degree of the (001) plane, could be cooled down to 82 K by pumping over a liquid nitrogen reservoir attached to the sample, heated to 1650 K for annealing, temperature stabilized to 0.5 degrees, or ramp its temperature via a resistive heating ac coupled routine. The temperature was monitored by means of a W5Re/W26Re thermocouple.

## 3. ADSORPTION OF $CD_3BR$ ON O/RU(001)

We found that by tuning the oxygen density above 0.25 ML, the orientation of adsorbed methyl bromide could be controlled bromine down or methyl down. Before discussing the interactions between $CD_3Br$ and adsorbed oxygen, the adsorption of oxygen on Ru(001) is briefly reviewed.

### *3.1 O/Ru(001)*

Oxygen dissociates on the ruthenium surface, and forms a strong chemical bond with the metal, as indicated by its high temperature of desorption (Fig. 1b). Since adsorbed oxygen hinders further oxygen dissociation, the sticking probability of oxygen decreases rapidly above 0.5 ML coverage. The plot of coverage vs. exposure in Fig. 1a indicates that at 5 Langmuir exposure the sticking probability (obtained by differentiating the curve in Fig. 1a) is 6 times lower than the initial sticking probability. Exposure to thousands of Langmuirs at 600 K is required in order to achieve a monolayer of oxygen.[17,18]

When an oxygen-covered surface with a coverage of 0.1–0.25 ML is annealed above 300 K, it forms an ordered (2 × 2)O-Ru(001) structure, which can be observed in LEED and was confirmed by STM measurements. Our LEED apparatus is rather insensitive to the coverage in this case (we are not able to monitor the spot intensity), since already at 0.1 ML coverage, small islands with the (2 × 2)O structure are formed. Above 0.25 ML coverage, domains of (2 × 1)O-Ru(001) are formed,[20,21] but this structure results in a LEED pattern similar to the (2 × 2)O because the domains do not have

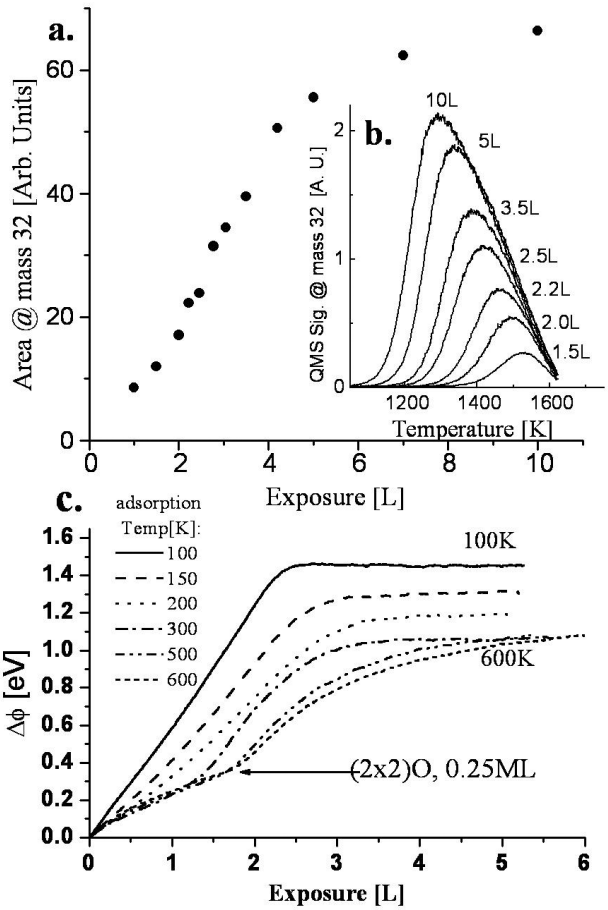


Fig. 1. (a) Integrated area under $O_2$ TPD peaks vs. exposure, indicating the diminishing sticking probability above 5 L. (b) ΔP-TPD of O/Ru(001) following adsorption of 1.5–25 L oxygen on Ru(001) at 600 K. (c) Δϕ vs. oxygen exposure at surface temperatures between 100 K and 600 K. At temperatures above 300 K, two distinct slopes are visible, before and after the completion of the ordered (2 × 2)O layer structure.

the same orientation. Therefore, another method was needed in order to calibrate the coverage.

Figure 1c presents the measured work function change during adsorption of oxygen at different temperatures. Above a sample temperature of 300 K at an exposure of about 2 L, a distinct change in slope is observed. This change was associated with the saturation of the $(2 \times 2)$O structure by Madey et al.,[22] but then it was believed to occur at 0.5 ML coverage. There is no such change at this exposure of the sticking probability (Fig. 1a), hence this change in slope is due to a 3 times larger dipole moment of the above-$(2 \times 2)$O-adsorbed oxygen. This change in dipole is probably due to the significant structure changes in the ruthenium top layers due to the adsorption of the first 0.25 ML of oxygen.[20, 21] These changes in structure also change the surface's reactivity, as will be discussed below.

We used the break in the $\Delta\phi$ slope as our coverage calibration point, with $2 \pm 0.2$ L exposure resulting in 0.25 ML coverage, and the TPD peak area plot as calibration to other oxygen exposures at 600 K.

### *3.2 The Interaction between $CD_3Br$ and Oxygen on Ru(001)*

Methyl bromide thermally dissociates on a clean Ru(001),[19] which results in adsorbed D atoms on the surface; thus the desorption of $D_2$ following $CD_3Br$ adsorption can be used as an indication of its dissociation. $D_2$ desorption in such an experiment, while gradually approaching an oxygen precoverage of $(2 \times 2)$O, is shown in Fig. 2. A coverage of 0.25 ML oxygen is enough to passivate the ruthenium surface and block the thermal dissociation channel of $CD_3Br$.

Gradually increasing the annealed oxygen pre-coverage above 0.25 ML and then covering it by 1.5 ML of $CD_3Br$ results in the $\Delta$P-TPD and differential $(d(\Delta\phi)/dT)$ $\Delta\Phi$-TPD spectra shown in Figs. 3 and 4. Three distinct peaks appear, denoted $\beta_1$, $\beta_2$, and $\alpha$. The relatively high temperature of the $\beta_1$ peak and its width were found by line shape analysis (not shown) to imply a binding energy of 17.8 kcal/mol of $CD_3Br$ molecules to the partly oxygen-covered surface, and a significant repulsive interaction among the adsorbates. The $\Delta\Phi$-TPD spectrum indicates that the $\beta_1$ molecules are adsorbed with their bromine end down towards the surface. The $\alpha$ peak at 120 K is due to molecules desorbing from the second layer, at a binding energy of 7.7 kcal/mol. As previously discussed in detail,[19] the second layer of $CD_3Br$ on the clean Ru(001) is adsorbed with its methyl end down. Increasing the oxygen coverage above 0.25 ML, towards local $(2 \times 1)$O-Ru(001)

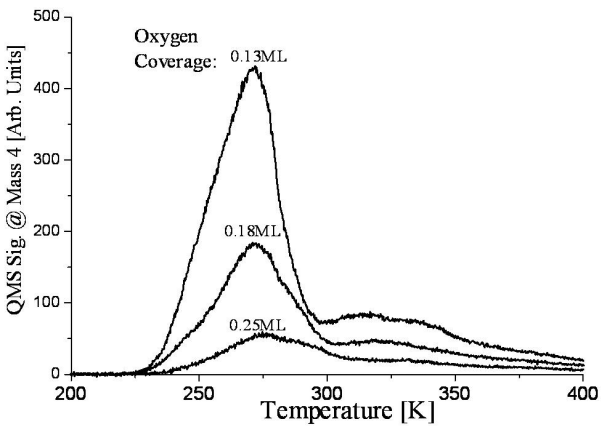


Fig. 2. $\Delta$P-TPD of $D_2$ recombinative desorption following adsorption of 2 ML $CD_3Br$ on different pre-coverages of annealed oxygen.

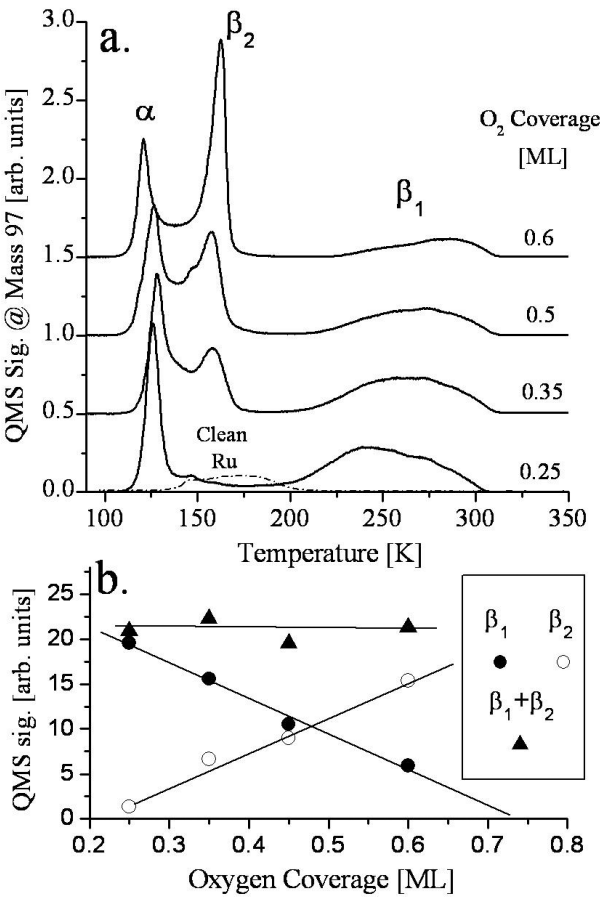


Fig. 3. (a) $\Delta$P-TPD of 1.5 ML of $CD_3Br$ on different oxygen pre-coverages over Ru(001). The heating rate was 2 K/s. As the oxygen coverage increases, the $CD_3Br$ molecules at the $\beta_1$ are shifted to the $\beta_2$ site. For comparison, desorption of 1 ML of $CD_3Br$ from the clean surface is shown as the dashed line. (b) The amount of $CD_3Br$ at the $\beta_1$ and $\beta_2$ sites as a function of oxygen coverage. The total coverage is constant.

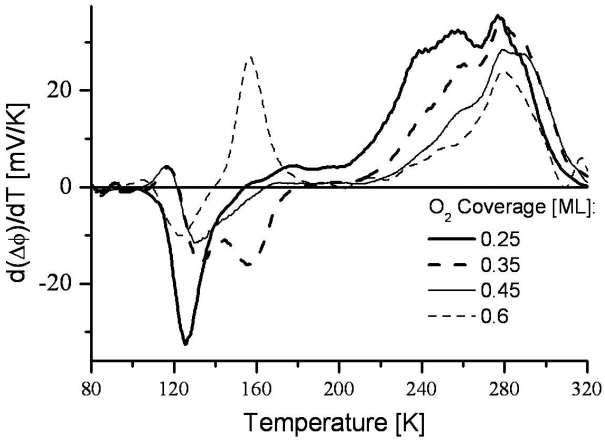


Fig. 4. Differential ΔΦ-TPD of 1.5 ML of $CD_3Br$ on different oxygen precoverages over Ru(001). The heating rate was 2 K/s. As the oxygen coverage increases, the $CD_3Br$ molecules at the $\beta_1$ are shifted to the $\beta_2$ site, and the $\beta_2$ site molecules change their orientation from methyl-down to bromine-down.

domains, creates a new adsorption site, $\beta_2$, which desorbs at 160 K (binding energy of 9.6 kcal/mol).

The total peak area of the methyl bromide ΔP-TPD spectra is invariant with oxygen coverage (indicating that the sticking probability of methyl bromide is insensitive to the oxygen coverage), as is the area of $\beta_1 + \beta_2$, to within 5% of our experimental uncertainty. The appearance of the $\beta_2$ molecules suggests that as the oxygen precoverage increases, $CD_3Br$ molecules are displaced from the $\beta_1$ adsorption sites into the $\beta_2$ sites. The interesting observation in Fig. 4 is that the *orientation* of the $\beta_2$ molecules is sensitive to the local surface density of adsorbed oxygen. This is inferred from the opposite sign of the relevant ΔΦ-TPD peak at 160 K. This is a justified interpretation of the work function change spectrum as long as no molecular dissociation takes place at this temperature. In fact, work function change measurements in the differential mode are expected to be more sensitive and relevant for the determination of overall molecular orientation with respect to the surface than, e.g., IR measurements. At oxygen coverages above 0.25 ML the $\beta_2$ molecules are arranged with their methyl down, while at 0.6 ML oxygen they are bromine down.

These orientation changes do not occur due to the heating ramp of the TPD, since the same orientations were observed by monitoring ΔΦ changes upon adsorption at 80 K (not shown here). As mentioned above, the first layer of $CD_3Br$ on the clean Ru(001) adsorbs in a bromine-down orientation, which results in a decrease of $\Delta\phi$ of about –2eV. When adsorbed on 0.6 ML of oxygen, two negative slopes are apparent, consistent with population of the $\beta_1$ (up to 0.6 L exposure) and subsequently the $\beta_2$ sites with bromine-down molecules. Adsorption of $CD_3Br$ on 0.35 ML of oxygen results in a decrease of $\Delta\phi$ up to exposure of 1.4 L (bromine-down $\beta_1$), then an increase in $\Delta\phi$ (methyl-down $\beta_2$).

A qualitative explanation for the flip in $\beta_2$ molecules is based on two effects: Local electrostatic interactions of the methyl bromide molecules with nearby adsorbed oxygen, combined with strong dipole–dipole interaction among neighboring $\beta_1$ molecules. At an oxygen precoverage of slightly more than 0.25 ML, when a $\beta_1$ molecule is displaced to a $\beta_2$ site, it becomes more weakly bound to the metal (desorption at 160 K instead of 240 K), and it is surrounded by neighboring $\beta_1$ molecules, aligned bromine-down on average. These $\beta_1$ neighbors induce the $\beta_2$ molecules to flip to the methyl-down configuration and lower the total energy of the system via attractive dipole–dipole attraction.[19] A similar hypothesis was proposed to explain the work function change data obtained from the coadsorption system of $K + H_2O$.[15,16] As the oxygen coverage increases, there are on average fewer $\beta_1$ neighbor molecules for each $\beta_2$ site, hence the $\beta_2$ molecules no longer flip. As a result of the presence of methyl-down molecules in the $\beta_2$ sites, bromine-down molecules are found in the second layer, as seen in the differential ΔΦ-TPD near 120 K (Fig. 4). The $\alpha$ peak in the differential work function spectrum is split between methyl-down (negative peak) and bromine-down (positive peak) orientations. At higher oxygen coverages, when no flipped $\beta_2$ exist, this $\alpha$ peak splitting is not detected anymore. These considerations are summarized in Fig. 5, as a schematic representation of the main interactions between the adsorbed molecules.

The number of oxygen atoms needed to shift one $CD_3Br$ molecule from a $\beta_1$ to a $\beta_2$ site can be estimated by plotting the total area of the $\beta_1$ peak vs. the total oxygen coverage (Fig. 3b). This plot indicates that adsorption of $0.75 \pm 0.05$ ML of oxygen should shift all of the $CD_3Br$ molecules. It was estimated that a full monolayer of $CD_3Br$ on the clean Ru(001) surface consists of $3.6 \pm 0.3 \times 10^{14}$ molecules/cm$^2$, which is about a quarter of the density of the ruthenium atoms. (1 ML of oxygen has the same surface density as the Ru(001).[21]) Therefore, while keeping 1 ML defined by the Ru(001) density, about a 0.5 ML of oxygen added to the 0.25 ML that forms the $(2 \times 2)$O structure shifts 0.25 ML of $CD_3Br$, suggesting that 2 oxygen atoms are necessary to shift 1 $CD_3Br$ to a $\beta_2$ site. Due to the small number of experimental points, and the fact that the surface density of $CD_3Br$ on the oxygen-covered surface may not be the

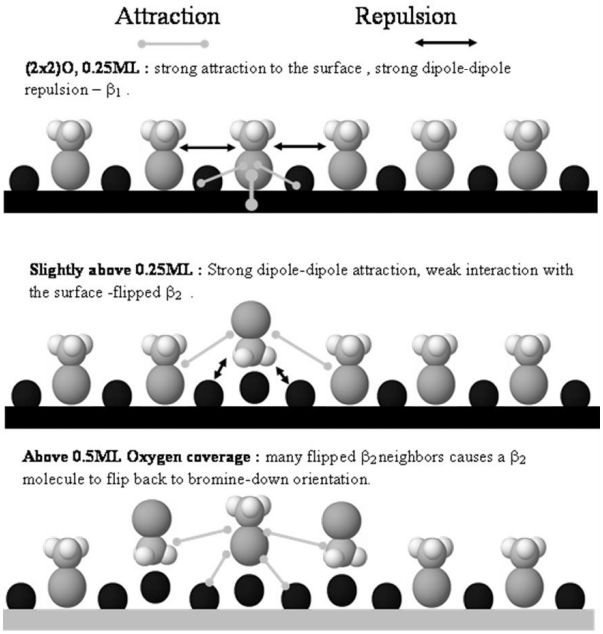


Fig. 5. An illustration of the proposed interactions between $CD_3Br$ and O/Ru(001), explaining the orientation changes of the $\beta_2$ molecules.

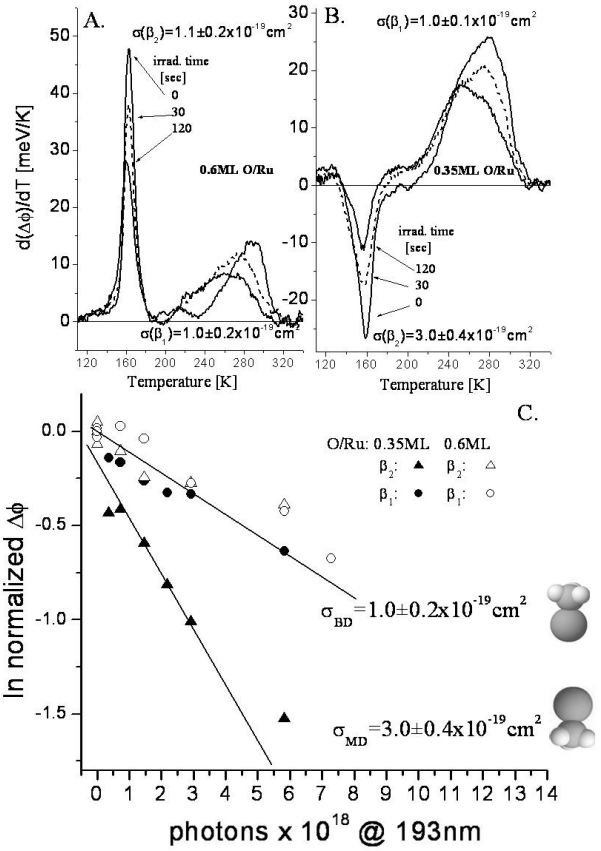


Fig. 6. ΔΦ-TPD of 0.8 ML of $CD_3Br$ adsorbed on 0.6 ML (a) and 0.35 ML (b) of oxygen, following different irradiation times by 193 nm UV laser irradiation. Photon flux was $2.4 \times 10^{16}$ photons/s at the sample. (c) The cross sections for depletion of the $\beta_1$ and $\beta_2$ peaks for the two oxygen coverages shown above. $\sigma_{BD} = 1.0 \pm 0.2 \times 10^{-19}$ cm$^2$ for all the $CD_3Br$ molecules that are oriented bromine-down (both $\beta_1$ and $\beta_2$), and $\sigma_{MD} = 3.0 \pm 0.4 \times 10^{-19}$ cm$^2$ for the methyl-down $\beta_2$ molecules.

same as on the clean Ru(001) surface, the possibility that 3 oxygen atoms are needed cannot be ruled out.

Once the ability to control molecular orientation has been confirmed, it becomes an ideal model system to examine the sensitivity of electron–molecule interaction to the molecular orientation by employing photo-mediated and direct electron-induced desorption and dissociation.

### 4. PHOTOCHEMISTRY OF $CD_3BR$/O/RU(001)

Differential ΔΦ-TPD spectra following 6.4 eV photon irradiation of 0.8 ML $CD_3Br$ adsorbed on 0.6 ML O/Ru are shown in Fig. 6a, for different irradiation times. The excimer laser power density at the sample was about 1 MW/cm$^2$ or $2.4 \times 10^{16}$ photons/s, a repetition rate of 50 Hz. The same experiments were performed at oxygen coverage of 0.35 ML (Fig. 6b). Both the $\beta_1$ and $\beta_2$ molecules undergo photoreaction, desorption, and fragmentation, which lead to an exponential decay of the relevant differential ΔΦ-TPD peak intensity. A plot of the logarithm of the integrated area under the d(Δφ)/dT spectra for both peaks vs. the number of photons should result in a linear plot. The initial slope of such plots determines the cross section for the photoreaction. In Fig. 6c such plots are presented.

The cross sections obtained this way can clearly be separated into two groups: The removal cross section of the $\beta_1$ molecules in both oxygen coverages and that of the $\beta_2$ molecules on top of 0.6 ML O/Ru coverage have a cross section ($\sigma$) of $(1.0 \pm 0.2) \cdot 10^{-19}$ cm$^2$. In contrast, the $\beta_2$ molecules that reside on top of 0.35 ML O/Ru, and are oriented methyl down, are removed at $\sigma = (3.0 \pm 0.4) \cdot 10^{-19}$ cm$^2$.

We find that molecules adsorbed at the same orientation (bromine down) but at different binding sites at different adsorption energies ($\beta_1$ and $\beta_2$ over 0.6 ML O/Ru, an 8.2 kcal/mol energy difference) possess the same overall removal (desorption + DEA) cross section. At the same time, the more weakly bound molecules that are flipped to the methyl-down configuration are

removed at a cross section that is three times larger. It is interesting to note that in spite of the different electronic configurations of the surface dictated by different oxygen coverage, the molecular orientations methyl-down and bromine-down within the $\beta_2$ sites are bound at exactly the same energy to the surface, as indicated by the TPD data in Fig. 3. This, we believe, emphasizes the dominance of the molecular orientation in determining the cross section for the (photo)-electron–molecule interaction. We cannot rule out, however, the possibility that the same factors that cause the molecular orientation changes, namely the dipolar interactions around the $\beta_2$ site, are also contributing to the difference in the cross section.

Orientation-dependent (photo)-electron–molecule interaction can be detected also by following the real-time desorption of $CD_3Br$ molecules during the UV irradiation. The QMS signal at mass 97 during continuous irradiation is shown in Fig. 7 (left), for the oxygen and $CD_3Br$ coverages discussed above. The cross section is extracted from the expression $I(t) = I(0)e^{-\sigma Ft}$, where I(t) is the QMS signal, F is the photon flux in photons/cm$^2$, and $\sigma$ is the photo-desorption cross section in cm$^2$. As before, only the initial $6 \times 10^{18}$ photons are considered. This is important in order to minimize the influence of photo-fragments on the tail of the decay curve.

The measured cross sections are $\sigma_{\text{Br Down}}$ ($\sigma_{\text{BD}}$) = $2.0 \pm 0.1 \times 10^{-19}$ cm$^2$ and $\sigma_{\text{Methyl Down}}$ ($\sigma_{\text{MD}}$) = $2.9 \pm 0.1 \times 10^{-19}$ cm$^2$ for the 0.6 ML and 0.35 ML O/Ru, respectively.

The QMS signal includes photo-desorption from both $\beta_1$ and $\beta_2$ sites, but it is insensitive to photo-fragmentation (DEA). The identical cross sections obtained by the real-time QMS detection and the work function change measurements are explained assuming that photo-electron mediated *desorption* is the dominant process in the methyl-down configuration (0.35 ML O/Ru). Dominance of electron-mediated *dissociative*

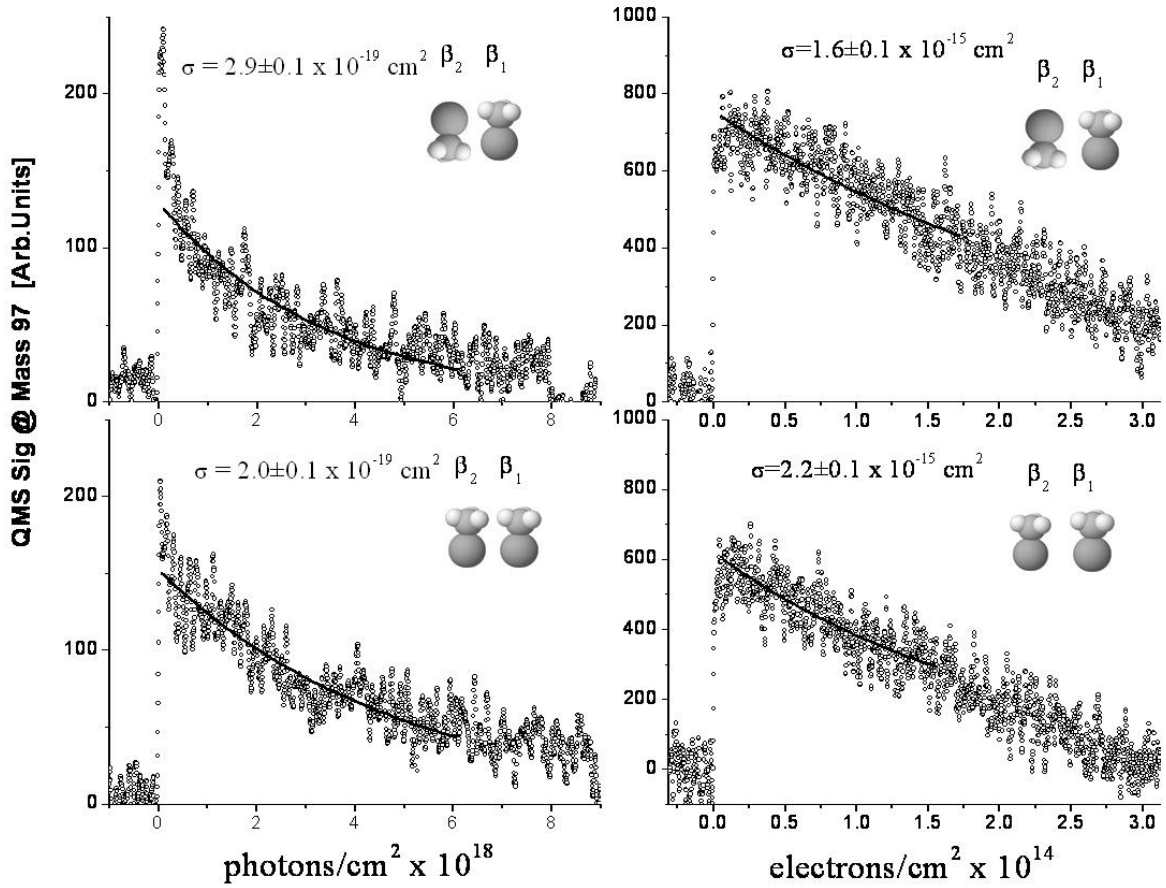


Fig. 7. QMS signal at mass 97 (open circles) during irradiation of 0.8 ML $CD_3Br$ on 0.35ML O/Ru(001) (*top*) and 0.6 ML O/Ru(001) (*bottom*). Irradiation was photo-electron generated from 193 nm photons (*left panels*) and direct 10 eV electrons from the gas phase, discussed in section 5, (*right panels*). The initial decay was fitted to an exponent (solid line) to extract the cross section for desorption.

channel in the methyl-down configuration of the $\beta_2$ molecules would have resulted in smaller integrated differential work function change near 160 K. This is due to the negative work function change contribution of both dissociation fragments, methyl and bromine,[19] if they adsorb on the surface. If fragments (e.g., methyl) are ejected to the gas phase, the overall work functions change and thus the measured cross sections are again expected to be similar to the electron-mediated parent molecular desorption. The fact that about $15 \pm 5\%$ of the parent molecules dissociate and their methyl fragments stay on the surface is established by the post-irradiation TPD of $D_2$ (and other products, see below), which is due to several consecutive photo-generated dissociation events of methyl and smaller fragments on the surface.

Post-irradiation stable molecular products that are observed by TPD are $CD_4$ (mass 20), $C_2D_6$ (mass 36), $D_2$ (mass 4), and mass 32 (tentatively assigned as $D_2CO$ based on comparison to ref 24). The yield of these photoproducts depends on the initial $CD_3Br$ surface coverage, as seen in Fig. 8.

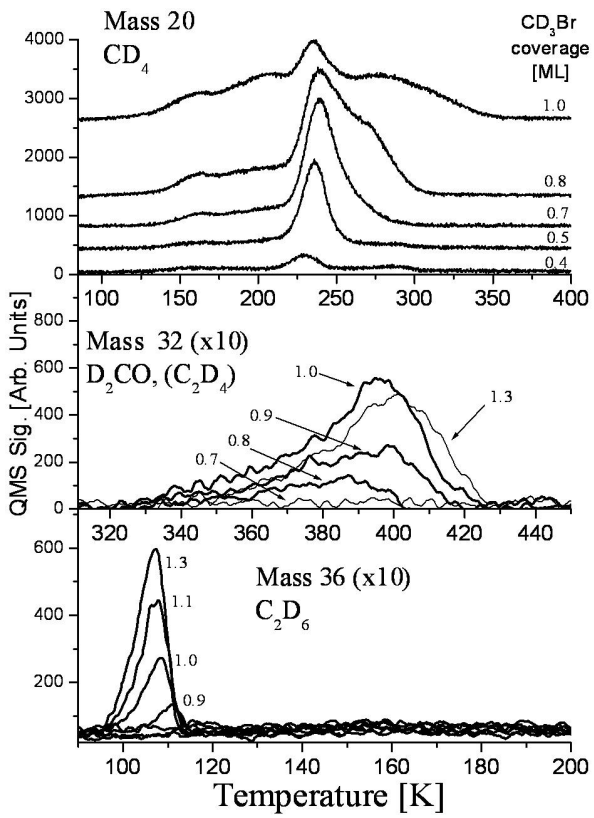


Fig. 8. ΔP-TPD of masses 20, 32, and 36, following adsorption of different amounts of $CD_3Br$ on 0.4 ML oxygen pre-covered Ru(001) and irradiation by $6 \times 10^{18}$ 193-nm photons. The $CD_3Br$ coverages are indicated on the graph in units of monolayers (ML).

The photoproducts that were produced after irradiation by $6 \times 10^{18}$ 193 nm photons (on a pre-coverage of 0.4 ML oxygen) were determined by scanning through masses 2–100 au during the TPD ramp. When the $CD_3Br$ coverage is gradually increased, a signal at mass 20 appears, and at higher coverage also at 32 and 36. This can be explained by considering the orientation and local environment of the molecules at each $CD_3Br$ coverage. Figure 9 shows a coverage-dependant TPD of $CD_3Br$ on 0.4 ML oxygen, revealing the gradual population of the $\beta_1$, $\beta_2$, and $\alpha$ peaks. Up to a $CD_3Br$ coverage of 0.5 ML, only the $\beta_1$ sites are populated. At coverages below 1 ML both $\beta_1$ and $\beta_2$ sites are populated, and above that coverage the $\alpha$ sites are also present. The yield of the products after irradiation of $6 \times 10^{18}$ photons (as determined by the integrated ΔP-TPD peak area in Fig. 8) is presented in Fig. 9. The remaining oxygen coverage is shown as well.

The formation of $C_2D_6$ becomes possible due to the presence of $\alpha$ molecules. Based on the scheme describing the adsorption sites (Fig. 9), the $C_2D_6$ formation is facilitated by the presence of neighbor methyl groups in the first and second layers that are oriented toward each other. The formation of $CD_4$, produced via surface recombinative desorption process of $CD_3 + D$, does not occur before population of the $\beta_2$ sites takes place. Photo-fragmentation of the $\beta_1$ molecules should lead to ejection to the gas phase of a methyl group, as indicated in the scheme of Fig. 9. Similar arguments suggest that dissociation of $\beta_2$ molecules should lead to the ejection of a bromine atom or negative ion, while the methyl group remains on the surface. Further photo-fragmentation of the methyl is the source of adsorbed D atoms, which thereafter lead to the formation of $CD_4$ upon ramping the surface temperature. Additional increase of the initial $CD_3Br$ coverage to populate the second layer ($\alpha$) decreases $CD_4$ production rate in spite of the fact that molecules are oriented methyl down. This is probably because it is not possible for the methyl from the second layer to stick and adsorb on the fully covered ($\beta_1 + \beta_2$) surface.

Methyl groups that are oriented toward the surface and thus strike it as a result of the DEA event can also react with the underlying oxygen atoms, as suggested both by the production of $D_2CO$, and by the depletion of the surface oxygen. This is observed starting at methyl bromide coverage of 0.7 ML. It is not fully understood yet why the oxygen abstraction reactions do not start right at the population onset of the $\beta_2$ site. Populating the second layer, however, does not seem to enhance or hinder the production of $D_2CO$.

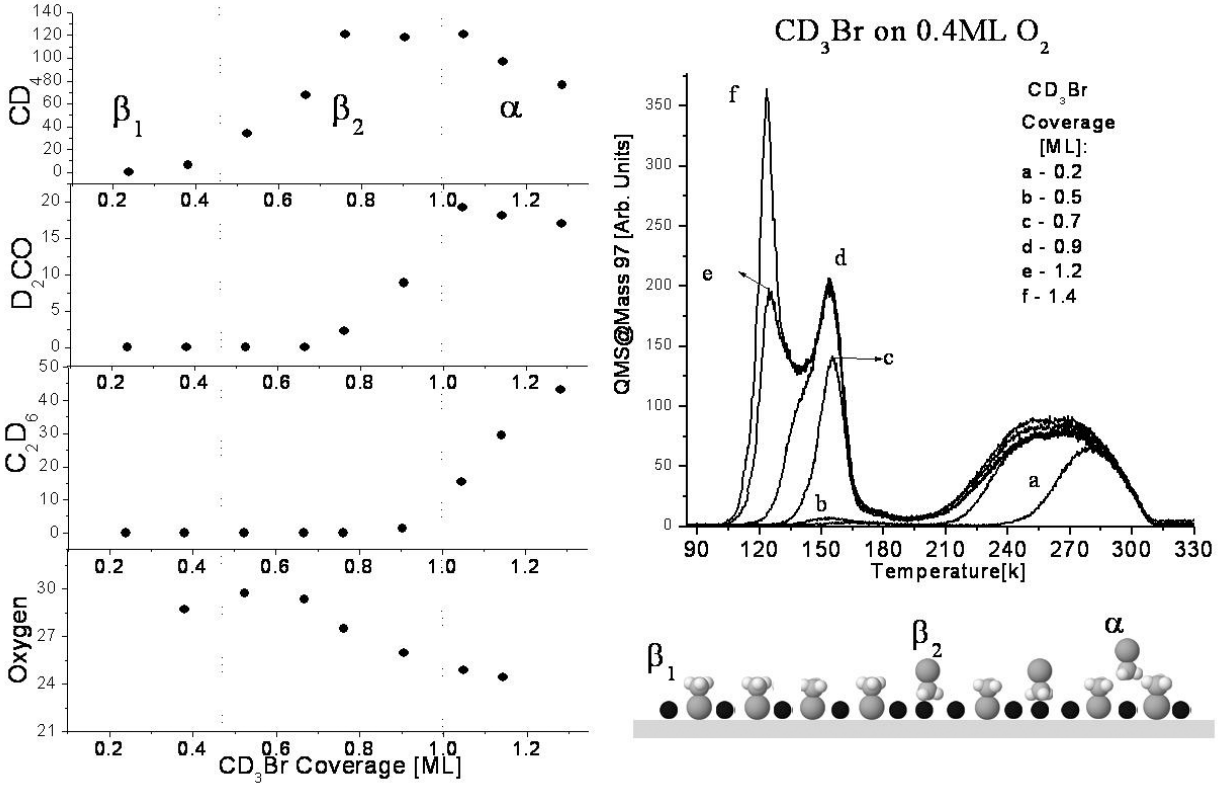


Fig. 9. The yields of the photoproducts and remaining oxygen after the irradiation conditions shown in Fig. 8, as a function of initial $CD_3Br$ coverage. To the right: ΔP-TPD of $CD_3Br$ showing the gradual population of the $\beta_1$, $\beta_2$, and $\alpha$ peaks with a scheme of these adsorption sites.

*4.1 Photo Hydro-Dehalogenation of $CD_3Br$*

The hydrodehalogenation[25] of halogenated aliphatic compounds is important as a way to clean hazardous solvents in industry, such as $CCl_4$. Both homogeneous[25] and heterogeneous[26] catalysis were employed for hydrodehalogenation, as was irradiation by UV light. The molecular details of these reactions are seldom understood. The photoreaction described above can be discussed as a model system for a simple hydrodehalogenation reaction[28] :

$$CD_3Br + D \xrightarrow{h\nu} CD_4 + Br$$

By utilizing the isothermal desorption analysis method discussed in detail in ref 27, we were able to extract for the first time the activation energy for the final step in the reaction, where adsorbed methyl photofragments and deuterium atoms recombine and desorb as methane.

The isothermal desorption signal of $CD_4$ following adsorption of 0.7 ML $CD_3Br$ on 0.4 ML O/Ru and irradiation by $6 \times 10^{18}$ 193-nm photons is shown in Fig. 10b for several temperatures. Briefly, plotting $1/\sqrt{QMS}$ vs. time for a second-order process results in a straight line (Fig. 10c) with a slope k′. This slope is proportional to the desorption rate, thus plotting ln k′ vs. 1/T should result in a linear plot (Fig. 10d).

Activation energy for the recombinative desorption reaction: $CD_3(ad) + D(ad) \rightarrow CD_4(g)$ ($E_{des}$) was determined from this plot to be 5.6 kcal/mol. This number most probably reflects the barrier for surface reaction. In contrast, activation barriers for the diffusion of methyl or deuterium fragments on a smooth surface such as Ru(001) are often smaller. In other words, if this had been a diffusion-limited surface reaction, it would have been detected at temperatures lower than 200 K.[28]

## 5. IRRADIATION BY 10 eV ELECTRONS

Real time desorption was measured also for irradiation with 10 eV electrons, as explained in the experimental section and demonstrated in Fig. 7 (*right panels*).

The cross sections for the electron-stimulated desorption (ESD) are four orders of magnitude larger than those for the photon-stimulated desorption (PSD). This

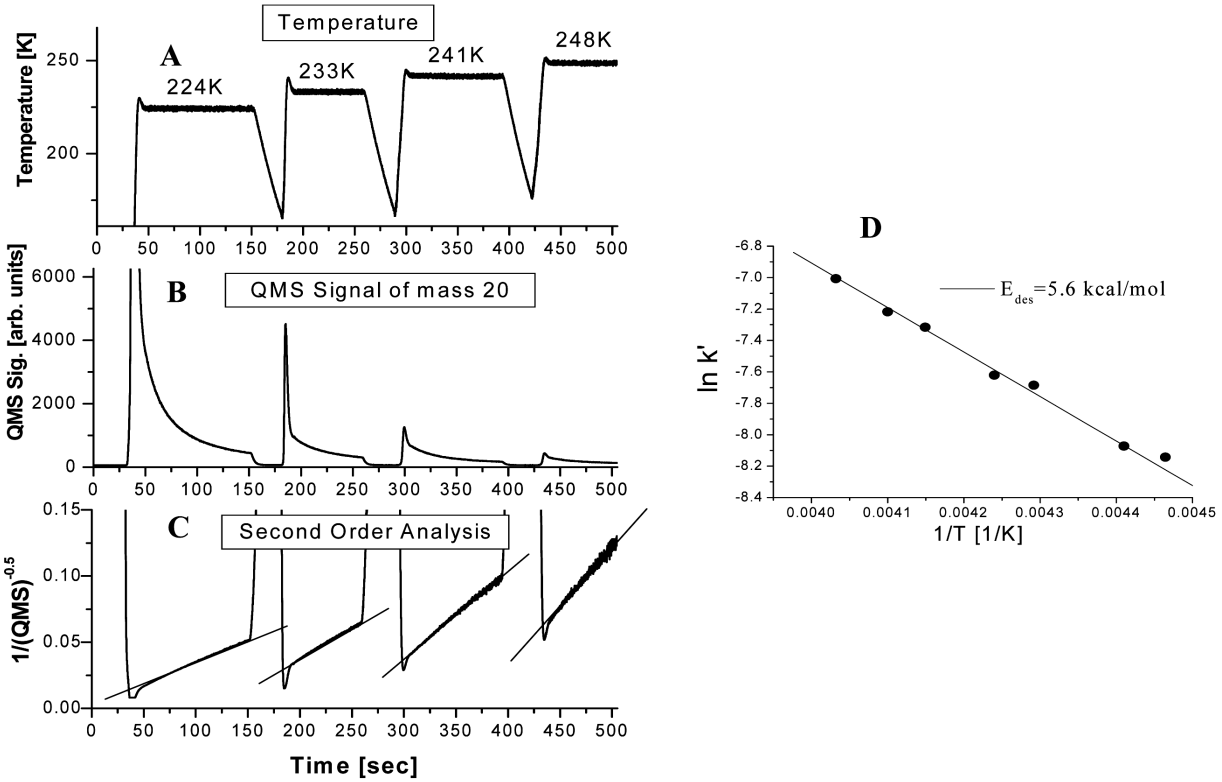


Fig. 10. Second-order isothermal desorption analysis of formation of $CD_4$. 0.7 ML $CD_3Br$ was adsorbed on 0.4 ML O/Ru and irradiated by $6 \times 10^{18}$ 193-nm photons. Temperatures of 224 K, 233 K, 241 K, and 248 K are shown. An activation energy of 5.6 kcal/mol was obtained by an Arrhenius plot.

large difference in magnitude was reported before for other systems, e.g., $NF_3$/Pt(111).[23] As in the PSD case, different cross sections are obtained for the different molecular orientations. The difference, however, has the opposite trend, namely the removal cross section of the methyl-down molecules is smaller than that of the bromine-down molecules. As in the PSD case discussed above, also here the difference in the cross section is attributed to electron–molecule steric effect, where the reaction $CD_3Br + e^-$ has a larger cross section when the electron approaches the molecule from the methyl end.

One should consider alternative mechanisms to explain the enhanced probability for both photo-induced and electron-induced desorption of methyl bromide from the O/Ru(001) surface when the methyl group faces the direction of approach of the electrons. One such explanation is the enhanced quenching rate at the bromine-down configuration. Such a mechanism may be justified if we consider that most of the negative charge resides on the bromine side of the adsorbed molecule following electron attachment. In this case, the larger charge density on the bromine side should overlap higher electron density of the metal when the bromine faces the surface, since it is closer to the surface than when it is in the methyl-down configuration. Larger charge density overlap often results in shorter excited-state lifetime or faster quenching back to the ground state. Shorter lifetime results, therefore, in a smaller probability for electron-induced desorption, as preliminary wave packet dynamical simulations indicate.[29] While this argument qualitatively explains the steric effect found in the photo-induced substrate-mediated desorption of methyl bromide at a photon energy of 6.4 eV, it cannot simultaneously rationalize the opposite steric effect found in the enhanced electron-stimulated desorption data. While it will be inaccurate to completely ignore the role of quenching, we tend to believe that kinematic (mass) effects lead to the larger photo-electron-induced desorption of the parent methyl bromide molecule when the methyl faces the substrate's surface.[29] The initial electron attachment step is probably also sensitive to the molecular orientation discussed in this work; however, its exact contribution is difficult to estimate.

## 6. PHOTOCHEMISTRY OF CAGED MOLECULES: $CO_2$@ICE

In the previous parts of this work the effect of local electrostatics among neighbor molecules on reorientation of adsorbates has been discussed. The photochemical consequences that result in the observation of steric effect in electron–molecule interaction were presented.[41] In this section we shall present another type of neighbor or environment effect on the organization and chemistry of molecules on surfaces. Here, the confinement of $CO_2$ molecules within a matrix of ice will be described, together with the resulting photo-excitation of such system.

As was demonstrated in several other molecular systems, $N_2$@Ice,[30] $CCl_4$@Ice,[31] $CH_3Cl$@Ice,[32] $CO_2$ is also compressed by post-adsorbed water molecules and eventually, as the water coverage increases beyond 25 bilayers (BL), this molecule becomes caged within the ice matrix—$CO_2$@Ice. This is demonstrated in Fig. 11, where the desorption temperature of $CO_2$ gradually shifts from 100 K when adsorbed in the absence of water to the typical explosive desorption that peaks at 165 K, 2 K in width, which coincides with the onset of $H_2O$ desorption from the "ice" layer.

A fraction of 0.18 of the full first layer of $CO_2$ thermally dissociates on clean Ru(001). This is determined from the ratio of the integrated TPD signal of $^{13}CO$ at mass 29 divided by the sum of integrated areas under the TPD signals at masses 29 and 45 ($^{13}CO_2$). Cage formation decreases the dissociation probability down to about half its value on the clean ruthenium surface. This is demonstrated in Fig. 12 by the decreasing TPD signal at mass 29. This observation may be rationalized by a shortage in vacant adsorption sites necessary to accommodate the dissociation products within the cage.

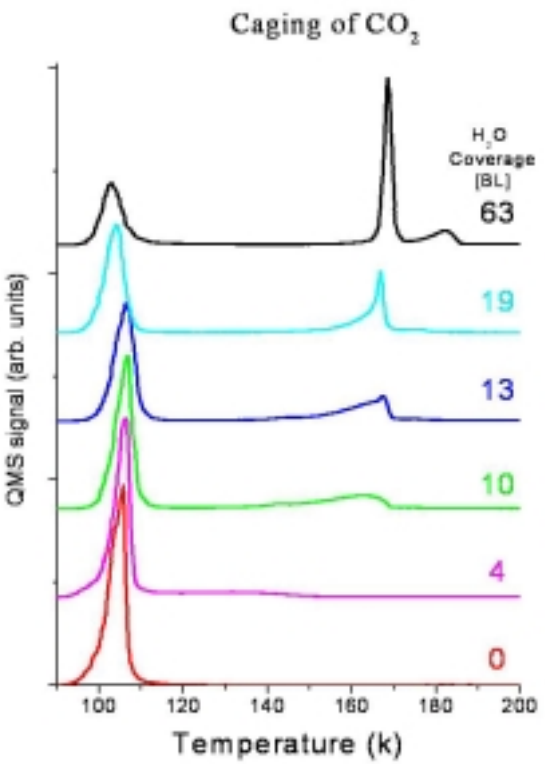


Fig. 11. TPD at mass 45 demonstrating the gradual caging of $^{13}CO_2$ under the indicated number of water bilayers (BL).

Exposing a monolayer of $CO_2$ adsorbed on clean Ru(001) to excimer laser irradiation at 193 nm results in photo-desorption and in enhanced dissociation. The dissociation channel is indicated by the gradual increase of mass 29 TPD signal at desorption temperature near 460 K, as a function of irradiation time. This is explained by an indirect substrate-mediated dissociative electron attachment (DEA) mechanism of $CO_2$. An excited $(CO_2)^-$ is momentarily formed following the laser irradiation, which subsequently dissociates to $CO_{ad}$ + $O_{ad}$ or it may undergo molecular desorption. The photo-desorption cross section for the parent carbon dioxide ($\sigma = 8 \cdot 10^{-21}$ cm$^2$) was measured by monitoring the mass 45 signal during irradiation, as shown in Fig. 13. The cross section for the competing photo-dissociation was determined to be five times smaller. Long irradiation times, however, result in the accumulation of more $^{13}CO$ products. 0.56 and 0.64 of the original 1 ML $^{13}CO_2$ has dissociated within the cage following 10 and 20 minutes irradiation times, respectively.

Upon irradiation of the caged $CO_2$ molecules by the 193-nm photons, however, a new reactivity channel opens up. In addition to photo-dissociation and photo-desorption of carbon dioxide, also water molecules partially dissociate. As a result, a new peak appears in the multi-mass TPD scan shown in Fig. 14. At mass 31, the desorption of formaldehyde is detected as a result of hot chemistry between $CO_2$ and water photo-fragments. It is impossible to determine at this point whether $H_2{}^{13}CO$ forms during a single excimer laser pulse or if this is the result of accumulated photo-products. Only 0.1 of the photo-dissociated carbon dioxide molecules undergo the reactivity channel of formaldehyde formation, which is about 0.01 of the initial parent molecule population. This product, however, is a unique consequence of the caged $CO_2$ in ice and cannot be formed otherwise.

## 7. CONCLUSIONS

In conclusion, we have discussed two cases of photochemistry of molecules constrained by their neighbor adsorbates. Steric effect has been identified and measured, for the first time, in the interaction of collimated (photo)-electrons with pre-oriented molecules. Control

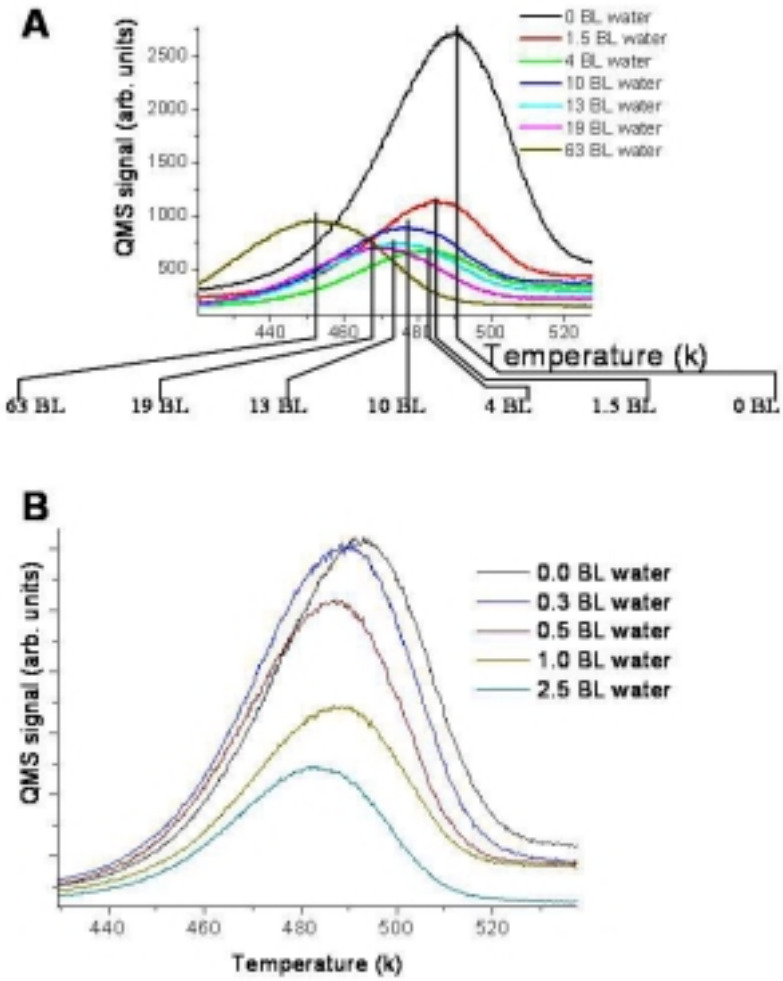


Fig. 12. TPD of $^{13}CO$ as a result of thermal dissociation of $^{13}CO_2$ on Ru(001). The decreasing signal is demonstrated as a function of the water layer thickness at thick (A) and thin (B) layers.

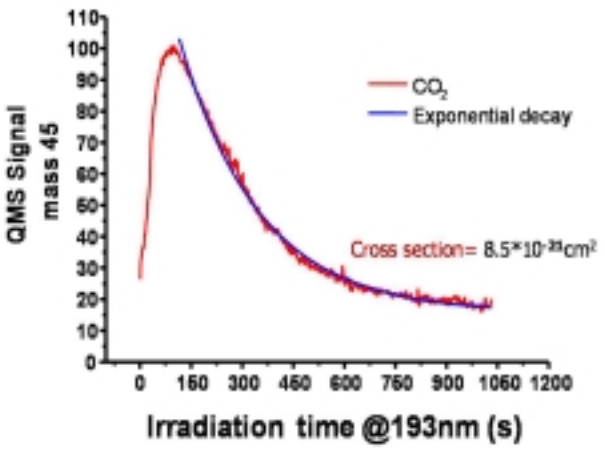


Fig. 13. Real-time detection and cross section extraction of photo-desorbing mass 45 during irradiation of $^{13}CO_2$/Ru(001) system by an excimer laser at 193 nm.

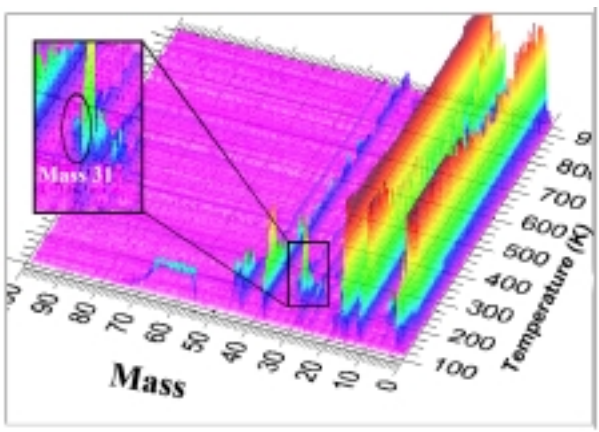


Fig. 14. A TPD taken simultaneously at all masses between 0–80 amu in a 3-D representation. The blow-up reveals the signal at mass 31 ($H_2{}^{13}CO$), which is the result of photochemistry of $CO_2$@Ice.

over the molecular orientation of adsorbed $CD_3Br$ was achieved by varying oxygen pre-coverage on Ru(001). When a flux of photo-electrons generated at the bulk metal strikes adsorbed methyl bromide from the methyl end, the overall electron-mediated reactivity has a cross section of $\sigma = 3.0 \cdot 10^{-19}$ cm$^2$, which is three times larger than the cross section determined for the BD-down configuration. Qualitatively similar results were obtained by direct bombardment with 10 eV electrons from the gas phase, but at cross sections that are four orders of magnitude larger.

The steric effect reported here is central to our basic understanding of electron transfer processes, which are among the most fundamental concepts in chemical reactivity.[33] Many biological systems function via a cascade of electron transfer processes, e.g., photosynthesis. Only in recent years has the detailed mutual structure of the complex molecular elements of photosystem-I been scrutinized by means of X-ray diffraction analysis of the relevant proteins.[34] Steric effects in such complex systems, if studied, may reveal some of the evolutionary steps that have led to a given structure over the others in plants and living organisms.

In the second example, $CO_2$ molecules were found to be trapped or caged within ice layers on Ru(001), $CO_2$@Ice. Caging has decreased thermal dissociation of carbon dioxide on the one hand, but also has produced new photochemical products upon irradiation at 193 nm. Formaldehyde at mass 31 ($H_2{}^{13}CO$) has been found as a new product, reported also to be formed in interstellar space, possibly under similar caging conditions of $CO_2$ within ice on solid grains.[35–40] The study of caged molecules under or within layers of ice under controlled experiments at UHV conditions is considered as a convenient and proper model for the formation of hydrocarbons in interstellar space. In space, layers of ice are known to accumulate on top of solid particles or grains together with other small molecules abundant in this low-temperature environment, such as carbon dioxide, ammonia, and CO, and then are exposed to UV and VUV light.[35–40] Integrated over a long time, new photochemical products (e.g., formaldehyde and other hydrocarbons) can be released if the grains are warmed up to the ice desorption temperature.

*Acknowledgments.* This work was partially supported by a grant from the United States-Israel Binational Science Foundation and by the Israel Science Foundation.

## REFERENCES AND NOTES

(1) Brooks, P.R. *Science* **1976**, *193*, 11.
(2) Parker, D.H.; Bernstein, R.B. *Annu. Rev. Chem. Phys.* **1989**, *40*, 561.
(3) Bernstein, R.B.; Herschbach, D.R.; Levine, R.D. *J. Phys. Chem.* **1987**, *91*, 5365.
(4) Parker, D.H.; Jalink, H.; Stolte, S. *J. Phys. Chem.* **1987**, *91*, 5427.
(5) Janssen, M.H.; Parker, D.H.; Stolte, S. *J. Phys. Chem.* **1991**, *95*, 8142.
(6) Marcus, R.A. *J. Chem. Phys.* **1965**, *43*, 679.
(7) Caron, L.G.; Perluzzo, G.; Bader, G.; Sanche, L. *Phys. Rev. B* **1985**, *33*, 3027.
(8) Naaman, R.; Haran, A.; Nitzan, A.; Evans, D.; Galperin, M. *J. Phys. Chem.* **1998**, *102(19)*, 3658.
(9) Ray, R.; Ananthavel, S.P.; Waldeck, D.H.; Naaman, R. *Science* **1999**, *283*, 814.
(10) Reed, M.A.; Zhou, C.; Muller, C.J.; Burgin, T.P.; Tour, J.M. *Science* **1997**, *278*, 252.
(11) Porath, D.; Bezryadin, A.; de Vries, S.; Dekker, C. *Nature* **2000**, *403*, 635.
(12) Sanche, L. *Scanning Microsc.* **1995**, *9*, 619.
(13) Negesha, K.; Fabrikant, I.I.; Sanche, L. *J. Chem. Phys.* **2001**, *114(11)*, 4934.
(14) Burrow, P.D.; Aflatooni, K. *J. Chem. Phys.* **2002**, *116(13)*, 5471.
(15) Bonzel, H.P.; Pirug, G.; Muller, J.E. *Phys. Rev. Lett.* **1987**, *58*, 2138.
(16) Muller, J.E. In *Physics and Chemistry of Alkali Metals Adsorption*; Bonzel, H.P.; Bradshaw, A.M.; Ertl, G., Eds.; Elsevier: Amsterdam, 1989, p 271.
(17) Kostov, K.L.; Gsell, M.; Jakob, P.; Moritz, T.; Widdra, W.; Menzel, D. *Surf. Sci. Lett.* **1997**, *394*, L138.
(18) Hoffmann, F.M.; Weizel, M.D.; Peden, C.H.F. *Surf. Sci.* **1989**, *253*, 59.
(19) Livneh, T.; Asscher, M. *J. Phys. Chem.* **1997**, *B101*, 7505.
(20) Lindroos, M.; Pfnur, H.; Held, G.; Menzel, D. *Surf. Sci.* **1989**, *222*, 451.
(21) Gsell, M.; Stichler, M.; Jakob, P.; Menzel, D. *Isr. J. Chem.* **1998**, *38*, 339.
(22) Madey, T.E.; Engelhardt, H.A.; Menzel, D. *Surf. Sci.* **1975**, *48*, 304.
(23) Junker, H.H.; White, J.M. *Surf. Sci.* **1997**, *382*, 67.
(24) Kis, A.; Kiss, J.; Solymosi, F. *Surf. Sci.* **2000**, *459*, 149.
(25) Alonso, F.; Beletskaya, I.P.; Yus, M. *Chem. Rev.* **2002**, *102*, 4009.
(26) Muftikian, R.; Fernando, Q.; Korte, N. *Water Res.* **1995**, *29*, 2434.
(27) Lilach, Y.; Danziger, I.M.; Asscher, M. *Catal. Lett.* **2001**, *76*, 35.
(28) Lin, J.-L.; Bent, B.E. *J. Phys. Chem.* **1992**, *96*, 8529.
(29) Jorgensen, S.; Zeiri, Y.; Asscher, M.; Lilach, Y.; Kosloff, R. *J. Phys. Chem. B* **2004**, *108*, 14056.
(30) Livneh, T.; Romm, L.; Asscher, M. *Surf. Sci.* **1996**, *315*, 250.
(31) Smith, R.S.; Huang, C.; Wong, E.K.L.; Kay, B.D. *Phys. Rev. Lett.* **1997**, *79*, 909.
(32) Lilach, Y.; Asscher, M. *J. Chem. Phys.* **2003**, *119(1)*, 407.
(33) (a) Kuznetsov, A.M. *Charge Transfer in Physics, Chemistry and Biology*; Gordon & Breach: New York, 1995. (b) In *Electron Transfer—From Isolated Mol-*

*ecules to Biomolecules*; Jortner, J.; Bixon, M., eds.; *Adv. Chem. Phys.* **1999**, *106*.

(34) (a) Krau, N.; Hinrichs, W.; Witt, I.; Fromme, P.; Pritzkow, W.; Dauter, Z.; Betzel, C.; Wilson, K.S.; Witt, H.T.; Saenger, W. *Nature* **1993**, *361*, 326. (b) Krau, N.; W.-D. Schubert, W.-D.; Klukas, O.; Fromme, P.; Witt, H.T.; Saenger, W. *Nature Struct. Biol.* **1996**, *3*, 965.

(35) (a) Whitten, D.C.B. *Origin Life Evol. B* **1997**, *27*, 249, and references therein. (b) Ehrenfreund, P.; Fraser, H. In *Solid State Astrochemistry*, NATO ASI series; Pirronello, V.; Krelowski, J., eds.; Kluwer Academic Publ.: 2003, pp 317–356.

(36) Scutte, W.A. *Adv. Space Res.* **1995**, *16(2)*, 53.

(37) Mumma, M.J.; Dello Russo, N.; DiSanti, M.A.; Magee-Sauer, K.; Novak, R.E.; Brittain, S.; Rettig, T.; McLean, I.S.; Reuter, D.C.; Xu, Li-H. *Science* **2001**, *292*, 1334.

(38) Agarwal, V.K.; Schutte, W.; Greenberg, J.M.; Ferris, J.P.; Briggs, R.; Conner, S.; Van De Bult, C.P.E.M.; Bass, F. *Origin Life Evol. B* **1985**, *16*, 21–40.

(39) Bernstein, M.P.; Dworkin, J.P.; Sandford, S.A.; Cooper, G.W.; Allamandola, L.J. *Nature* **2002**, *416*, 401.

(40) Munoz Caro, G.M. *Nature* **2002**, *416*, 403.

(41) Lilach, Y.; Asscher, M. *J. Phys. Chem. B* **2004**, *108*, 4358.